MULTIPATH GHOST CORRELATION-BASED NLOS TARGET LOCALIZATION AND BUILDING LAYUOT ESTIMATION

Yufei Wei[1], Shisheng Guo[*,1,2], Zihan Xu[1], Xu Hao[1], Zhihao Zhu[1], Yupeng Yu[1], Yisen Zhou[1], Guolong Cui[1,2]
[1]*School of Information and Communication Engineering*
University of Electronic Science and Technology of China, Chengdu, China
[2]*Yangtze Delta Region Institute (Quzhou)*
University of Electronic Science and Technology of China, Quzhou, China
*Email: ssguo@uestc.edu.cn

***Abstract*—This paper considers the problem of jointly estimating target locations and reconstructing building layouts in non-line-of-sight (NLOS) scenarios. The proposed method employs Range-Doppler (RD) features for multipath separation to extract time of arrival (TOA) information, followed by the Iterative Adaptive Approach (IAA) to determine the direction of arrival (DOA) and estimate multipath ghost positions. By utilizing the spatial correlation between multipath ghosts and building layout, the algorithm determines the optimal candidate target locations and wall parameters through spatial matching. The feasibility of NLOS target precise localization and building layout estimation is demonstrated by Electromagnetic (EM) simulations results.**

***Index Terms*—NLOS target detection, Building layout estimation, Multipath ghost correlation, Space matching**

I. Introduction

Recently, non-line-of-sight (NLOS) sensing technology, which extends the detection range and enables the detection of hidden targets, has become essential in fields such as counterterrorism and autonomous driving, attracting significant attention. [1]–[3].

Hindered by obstructions, traditional line-of-sight (LOS) methods fail to detect targets effectively. In contrast, NLOS sensing technology leverages electromagnetic (EM) wave properties and multipath propagation to detect targets. A track-before-detect (TBD) method introduced in [4] addresses the challenge of detecting NLOS targets but lacks high localization accuracy. To achieve more accurate localization performance, several NLOS target localization methods inspired by techniques used in indoor multipath ghost suppression have been proposed. An imaging dictionary fusion algorithm was proposed in [5], utilizing NLOS sub-images generated from each propagation path and integrating them through a multiplicative fusion process to accurately locate multiple targets. Additionally, a grid-matching-based NLOS localization approach proposed in [6] computes the time of arrivals (TOAs) for each grid based on the multipath propagation model and selects the grid that best matches the arrival time of the round-trip multipath echo measurement, thereby improving the accuracy of NLOS target localization.

However, the performance of the aforementioned methods heavily relies on prior knowledge of the building layout. In the absence of such knowledge, their accuracy significantly deteriorates or even fails entirely. To overcome this limitation, Chen *et al.* [7] proposed a sparse-driven joint estimation method that integrates the morphological reshaping group sparse constraint (SR-GSC) algorithm with the particle swarm optimization (PSO) method to simultaneously reconstruct unknown building layouts and target locations. Furthermore, Xue *et al.* [8] proposed an elliptic envelope approximation (EEA) algorithm for the localization of the NLOS target and the reconstruction of the building layout in complex geometric environments. This method addresses the limitations of high scene regularity and the lack of a multipath complementary mechanism in existing approaches. However, it is restricted to the localization of a single target. Moreover, these methods still assume the LOS wall parameters are known, making them ineffective when this information is unavailable. Consequently, to ensure robust performance in practical scenarios, it is essential to simultaneously estimate the positions and angles of both LOS and NLOS walls.

In this paper, we propose a novel algorithm that leverages the spatial correlation among different multipath ghosts to jointly estimate the target location and reconstruct the building layout, including both NLOS and LOS walls. Initially, the method separates multipaths using Range-Doppler (RD) topological features to determine the TOA for each path. Subsequently, the iterative adaptive approach (IAA) is employed to extract the direction of arrival (DOA) for these multipaths, facilitating the estimation of multipath ghost positions. Furthermore, by exploiting the geometric relationship between multipath ghosts and the building layout, the algorithm iteratively refines candidate target locations and updates wall parameters through spatial matching until an optimal solution

This work was supported in part by the National Natural Science Foundation of China under Grant 62371110, in part by the 111 Project under Grant B17008, in part by the Municipal Government of Quzhou under Grant 2023D032. (*Corresponding author: Shisheng Guo.*)

satisfying spatial constraints is found. Finally, EM simulations validate the effectiveness of the proposed method.

II. Multipath Propagation Model

Consider an NLOS scenario consisting of three walls, as illustrated in Fig. 1. Surface-1 and Surface-2 form an angle denoted as θ_1, while Surface-3 forms an angle θ_2 with the x-axis. The Multiple-Input Multiple-Output (MIMO) radar system comprises M transmitters and N receivers, positioned near Surface-1 to detect the concealed targets. Thus, the echo of the k-th frame $y_{mn}^k(t)$ received by the n-th receiving antenna, after being reflected and diffracted from the signal $s(t)$ transmitted by the m-th transmitting antenna, can be expressed as

$$\begin{aligned} y_{mn}^k(t) = &\sum_{p,q} \sigma_{m,p}^{i,k}\sigma_{n,q}^{i,k} a_T(\theta_{m,p}^i) a_R(\theta_{n,q}^i) \\ &\times s(t-\tau_{m,p}^{i,k}-\tau_{n,q}^{i,k}) + \xi^k(t) + \eta^k(t), \\ &i = 1,2,\ldots,I, k = 1,2,\ldots,K, \end{aligned} \tag{1}$$

where p represents the transmitting path, q represents the receiving path, σ^i is the attenuation factor of the i-th target, and τ is the propagation time delay. The corresponding values $a_T(\theta_m^i)$ and $a_R(\theta_n^i)$ of the transmitting and receiving antennas in the steering vectors are expressed as

$$\begin{aligned} a_T(\theta_m^i) &= e^{j\frac{2\pi d_T \sin(\theta_m^i)}{\lambda}(m-1)}, \\ a_R(\theta_n^i) &= e^{j\frac{2\pi d_R \sin(\theta_n^i)}{\lambda}(n-1)}, \end{aligned} \tag{2}$$

where d_T represents the interval between adjacent transmitting antennas, and d_R represents the interval between adjacent receiving antennas. θ_m^i and θ_n^i denote the angle of departure and arrival, respectively. $\xi(t)$ denotes the signal that combines the direct path and the reflection path from obstacles such as walls. $\eta(t)$ accounts for the ambient noise.

Without loss of generality, we assume that there is a single target located at (x_t, y_t) in the NLOS region, denoted by $\boldsymbol{Q}$. Considering propagation losses, EM waves reach the target through diffraction path, first-order reflection path, second-order reflection path and their combined paths as depicted in Fig. 1. The virtual target positions corresponding to these multipaths are denoted as $\boldsymbol{Q}_{00}$ - $\boldsymbol{Q}_{22}$. Specifically, the position of the equivalent virtual target $\boldsymbol{Q}_{00}$, associated with the diffraction path, is given by

$$\boldsymbol{Q}_{00} = [x_0, y_0]^T = \left\{(x-x_c)^2 + (y-y_c)^2 = \|\boldsymbol{CQ}\|_2^2\right\}, \tag{3}$$

where (x_c, y_c) is the position of corner C, and $\|\boldsymbol{CQ}\|_2$ is the distance from the target to the corner, $\|\cdot\|_2$ represent is the ℓ_2-norm. For the reflection path, the position of the virtual target is related to the position and angle of Surface-2 and Surface-3. The Householder transformation is introduced to determine the mirror position. Before that, the surface is defined by the linear equation $x\cos\theta_h - y\sin\theta_h + d_h = 0$, where θ_h is the angle between Surface-h and the positive direction of the x-axis, and d is the perpendicular distance from the origin to Surface-h, $h \in \{2,3\}$. Thus, the linear equation is converted into

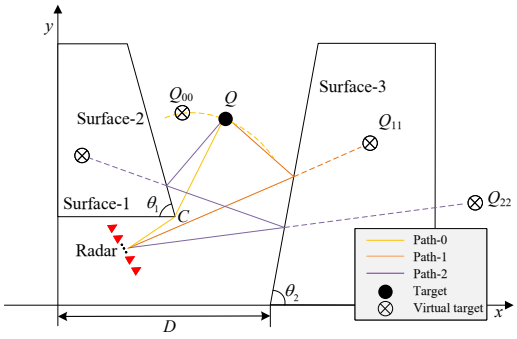

Fig. 1. Multipath propagation in a NLOS scenario

$\overline{\boldsymbol{a}}_{\boldsymbol{h}}^{\boldsymbol{T}}\overline{\boldsymbol{x}} = 0$, where $\overline{\boldsymbol{a}}_{\boldsymbol{h}} = [\boldsymbol{a_h}, d_h]^T$, $\boldsymbol{a}_h = [\cos\theta_h, -\sin\theta_h]^T$, $\overline{\boldsymbol{x}} = [x, y, 1]^T$, and T is the transpose operator. Consequently,, the virtual position of the target with respect to Surface-h, relative to the Householder matrix $\mathbf{P_h}$, can be determined by

$$\boldsymbol{x'} = \mathbf{P_h}\boldsymbol{x} - 2d_h, \tag{4}$$

where

$$\mathbf{P_h} = \mathbf{I} - 2\frac{\boldsymbol{a}_h\boldsymbol{a}_h^T}{\|\boldsymbol{a}_h\|^2}, \tag{5}$$

with $\mathbf{I}, \boldsymbol{x}, \boldsymbol{x'}$, respectively, the identity matrix, the actual position and mirror position with respect to Surface-h. Based on the Householder transformation, the virtual positions with respect to the multiple reflection paths can be determined by

$$\begin{cases} \boldsymbol{Q}_{11} = [x_1, y_1]^T = \mathbf{P_3}\boldsymbol{Q} - 2d_3 \\ \boldsymbol{Q}_{22} = [x_2, y_2]^T = \mathbf{P_3}\left(\mathbf{P_2}\boldsymbol{Q} - 2d_2\right) - 2d_3. \end{cases} \tag{6}$$

Based on the positions of the virtual targets, the single-trip time delay $\tau_{m,p}$ along the p-th path for the m-th transmitter and $\tau_{n,q}$ along the q-th path for the n-th receiver can be calculated as follows

$$\tau_{m,p} = \begin{cases} (\|\mathbf{T}_m\boldsymbol{C}\| + \|\boldsymbol{CQ}\|)/c, & p = 0, \\ \|\mathbf{T}_m\boldsymbol{Q}_{pp}\|/c, & p = 1,2, \end{cases} \tag{7}$$

$$\tau_{n,q} = \begin{cases} (\|\mathbf{R}_n\boldsymbol{C}\| + \|\boldsymbol{CQ}\|)/c, & q = 0, \\ \|\mathbf{R}_n\boldsymbol{Q}_{qq}\|/c, & q = 1,2, \end{cases} \tag{8}$$

where c is the speed of light, $\mathbf{T}_m$ and $\mathbf{R}_n$ are the position of the m-th transmitter and the n-th receiver, respectively. Therefore, the corresponding round-trip time delay is given by

$$\tau = \tau_{m,p} + \tau_{n,q} \quad p,q \in \{0,1,2\}. \tag{9}$$

Based on the multipath model, a joint estimation algorithm of building layout and target will be proposed in Section III.

III. Joint Estimation Algorithm of Buliding Layout and NLOS Target

This section introduces the proposed algorithm for joint estimation of building layout and NLOS targets, enabling building layout reconstruction with fewer constraints. The method comprises three main steps: multipath recognition based multi-domain features, multipath ghost position extraction, followed by building layout and target positions estimation.

A. Multipath Recognition Based on Range-Doppler Features

By leveraging the topological relationships in the RD spectrum, the recognition strategy described in [9] can identify six types of paths including diffraction paths, first-order reflection paths, second-order reflection paths, and their respective combination paths. This paper employs this method to achieve multipath recognition. These paths, denoted as P_{00}, P_{10}, P_{11}, P_{12}, P_{02}, and P_{22}, form a triangular structure in the RD map, which is clearly illustrated in Fig. 3(a). Among them, the three round-trip paths are located at the vertices of the triangle, while their combined paths are positioned at the midpoints of the three edges. The recognition results of the K frames are stored in the path utilization vector, and the path utilization vector for the i-th target is represented as

$$\mathbf{G}_u^i = \begin{bmatrix} d_{00}^{1,i} & d_{11}^{1,i} & d_{22}^{1,i} \\ d_{00}^{2,i} & d_{11}^{2,i} & d_{22}^{2,i} \\ \vdots & \vdots & \vdots \\ d_{00}^{K,i} & d_{11}^{K,i} & d_{22}^{K,i} \end{bmatrix}, i = 1, 2, ..., I, \tag{10}$$

where $d_{00}^{k,i}, d_{11}^{k,i}, d_{22}^{k,i}$ represent the distance information of the diffraction path, first-order multipath, and second-order multipath detected in the k-th frame for the i-th target, respectively. Based on the identified multipath components, the corresponding ghost positions can be inferred.

B. Multipath Ghost Position Extraction

The path identification results based on the RD spectrum include only the distance and Doppler information of the corresponding paths. To extract the exact locations of the multipath ghost targets, the corresponding angle information is also required. In this paper, the iterative adaptive approach (IAA) in [10] is implemented to obtain angle information. Applying the IAA method to each extracted path provides the corresponding angle information, which is then integrated into the angle matrix J. The angle matrix for the i-th target is represented as

$$\mathbf{J}_u^i = \begin{bmatrix} \theta_{00}^{1,i} & \theta_{11}^{1,i} & \theta_{22}^{1,i} \\ \theta_{00}^{2,i} & \theta_{11}^{2,i} & \theta_{22}^{2,i} \\ \vdots & \vdots & \vdots \\ \theta_{00}^{K,i} & \theta_{11}^{K,i} & \theta_{22}^{K,i} \end{bmatrix}, i = 1, 2, ..., I, \tag{11}$$

where $\theta^{k,i}$ denotes the angles of the different paths in the k-th frame.

After obtaining the distance and angle of different multipath ghosts, the exact location of the multipath ghosts can be confirmed. It should be noted that EM waves turn at corners during diffraction, so it is not possible to determine the position of diffracted ghosts by the angle of arrival of the diffraction path. Therefore, only first-order and second-order ghosts are considered in this section, which can be expressed as

$$\begin{cases} \boldsymbol{Q}_{11}^{k,i} = [x_1, y_1]^T = [d_{11}^{k,i} \cos\theta_{11}^{k,i} + x_R, d_{11}^{k,i} \sin\theta_{11}^{k,i} + y_R]^T \\ \boldsymbol{Q}_{22}^{k,i} = [x_2, y_2]^T = [d_{22}^{k,i} \cos\theta_{22}^{k,i} + x_R, d_{22}^{k,i} \sin\theta_{22}^{k,i} + y_R]^T \end{cases}, \tag{12}$$

where (x_R, y_R) is the position of radar antenna array center. $\boldsymbol{Q}_{11}^{k,i}, \boldsymbol{Q}_{22}^{k,i}$ denote the estimated first-order ghost and second-order ghost positions of the i-th target in the k-th frame, respectively.

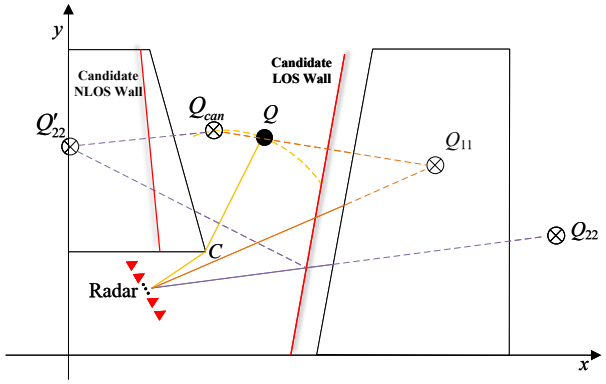

Fig. 2. Spatial correlation among multipath ghosts, candidate target and candidate walls

C. Building Layout and Target Parameters Estimation

As discussed in Section II, the positions of multipath ghosts are determined by both the building layout and the target position. Therefore, its spatial correlation feature, which describes the symmetric relationships among ghosts, targets, and walls as shown in Fig. 2, can be leveraged to determine the optimal target location and building layout parameters that satisfy the wall corner constraint.

The corner C can be estimated by the method in [11]. Based on the distance of the diffraction path and the position of the wall corner, it can be determined that the target is located on a circular arc centered on the wall corner. Set the angle search interval as $\theta = [\theta_1, ..., \theta_H]^T$, each angle corresponds to a candidate target position, denoted as

$$\boldsymbol{Q}_{can} = [x_{can}, y_{can}]^T = [d_{CQ} \cos\theta_h + x_C, d_{CQ} \sin\theta_h + y_C]^T, \tag{13}$$

where d_{CQ} is the diffraction path length minus the distance from the radar to the corner of the wall, $[x_C, y_C]$ is the position coordinates of the corner of the wall, and θ is all possible angles of the target. By traversing all angles, all candidate targets can be obtained.

For each candidate target, the specific parameters of the corresponding candidate wall can be determined by solving an inverse problem that incorporates the positions of the first-order and second-order ghost targets. Based on the spatial correlation between the candidate target and the first-order

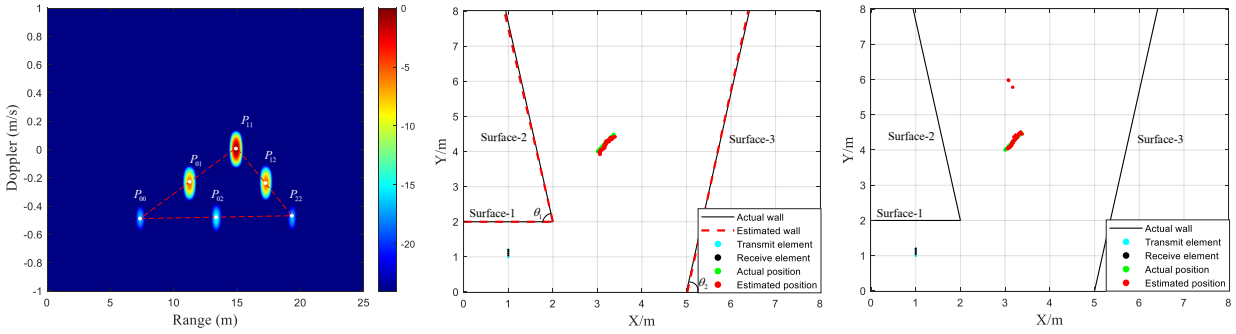

(a) (b) (c)

Fig. 3. Simulation results of a single target moving along a straight route. (a) RD Map, (b)Target localization result, NLOS wall and LOS wall estimation result obtained by using the proposed algorithm, and (c) Target localization results obtained by using GMM.

ghost, the candidate LOS wall surface, Surface-3, corresponds to the perpendicular bisector of the line segment connecting points $\boldsymbol{Q}_{11}$ and $\boldsymbol{Q}_{can}$. The slope of this bisector w_{LOS} is given by

$$w_{LOS} = -\frac{x_{can} - x_{11}}{y_{can} - y_{11}}, \tag{14}$$

and it passes through the midpoint

$$(\frac{x_{can} + x_{11}}{2}, \frac{y_{can} + y_{11}}{2}). \tag{15}$$

After determining the linear equation of the candidate LOS wall, from the spatial correlation between the candidate LOS wall and the second-order ghost, the symmetry point of the candidate target with respect to the candidate NLOS wall can be found as

$$\boldsymbol{Q}_{22}^{'} = \left[x_{22}^{'}, y_{22}^{'}\right]^{T}, \tag{16}$$

where $\boldsymbol{Q}_{22}^{'}$ needs to satisfy the following constraints

$$w_{LOS} = -\frac{x'_{22} - x_{22}}{y'_{22} - y_{22}} = \frac{(y_{can} + y_{11}) - (y_{22} + y'_{22})}{(x_{can} + x_{11}) - (x_{22} + x'_{22})}. \tag{17}$$

Similarly, the candidate NLOS wall corresponds to the perpendicular bisector of the line segment connecting $\boldsymbol{Q}_{22}^{'}$ and $\boldsymbol{Q}_{can}$. The slope of this bisector is given by

$$w_{NLOS} = -\frac{x_{can} - x'_{22}}{y_{can} - y'_{22}}, \tag{18}$$

and it passes through the midpoint

$$(\frac{x_{can} + x'_{22}}{2}, \frac{y_{can} + y'_{22}}{2}). \tag{19}$$

Since the wall corner position must lie on the NLOS wall, a wall corner position constraint can be introduced as a decision criterion. Specifically, by traversing all candidate NLOS walls, if the wall corner lies on a candidate NLOS wall, spatial location matching is considered successful. In this case, the candidate NLOS wall is identified as the actual NLOS wall, the candidate LOS wall is regarded as the actual LOS wall, and the candidate target location is recognized as the actual target position. This process simultaneously achieves NLOS target localization and building layout reconstruction.

IV. Simulation Results

This section presents the EM simulation results based on the EM simulation software gprmax [12] using the Finite Difference Time Domain (FDTD) method to verify the feasibility of the proposed algorithm. The corner scenario is depicted in Fig. 1. The simulation scenario is an 8m $\times$ 8m area, where the corner is positioned at (1.00 m, 1.00 m), and Surface 3 intersects the x-axis at $x = 5$m. Surface-1 and Surface-2 form an angle denoted as $\theta_1 = 80°$, while Surface-3 makes an angle $\theta_2 = 80°$ with the x-axis. To detect the targets, a MIMO array with two transmitters and four receivers is employed. The transmitters are positioned at (1.00 m, 1.00 m) and (1.00 m, 1.20 m), while the receivers are placed at equal intervals of 0.05 m. A step-frequency signal with a center frequency of f_c = 3 GHz and a bandwidth of B = 1 GHz is used as the transmitting signal. A total of 50 frames of data are generated in this simulation.

A. Single Target Moves Along A Straight Route

Assume that the target moves along a linear path from (3.00 m, 4.00 m) to (3.37 m, 4.49 m). A 2D FFT is applied to the echo signal after background clutter removal, generating an RD plot at a signal-to-noise ratio (SNR) of 20 dB, as shown in Fig. 3(a). As analyzed in Section III, the six main multipaths associated with a single target exhibit a strong geometric relationship in the RD spectrogram. After obtaining the path identification results, the proposed method further estimates the target location and reconstructs the building layout. The target localization and building layout reconstruction results obtained using the proposed method are presented in Fig. 3(b).

To validate the feasibility of the algorithm, localization results using the grid-matching method (GMM) [6] are shown in Fig. 3(c), and the root mean square error (RMSE) [13] is introduced to evaluate its performance. The horizontal coordinate of the LOS wall's intersection with the x-axis is used as a reference for determining its location. At an SNR of 20 dB, the RMSE for 50 frames is 0.06 m. The LOS wall position is estimated as 5.01 m with an RMSE of 0.01 m. The LOS wall angle is 80.31°, with an RMSE of 0.31°, while the NLOS wall angle is 79.70°, with an RMSE of 0.30°. Since the GMM method requires prior knowledge of the building scene,

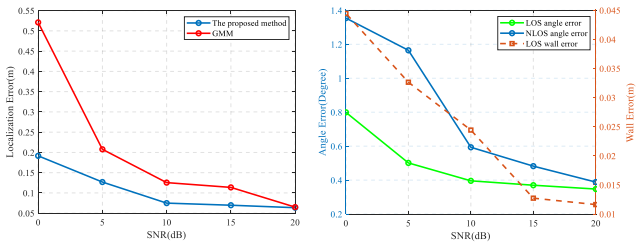

(a) (b)

Fig. 4. Relationship between parameter estimation error and SNR. (a) Localization error of different algorithms and (b) Angle error of LOS and NLOS walls and positional error of LOS walls.

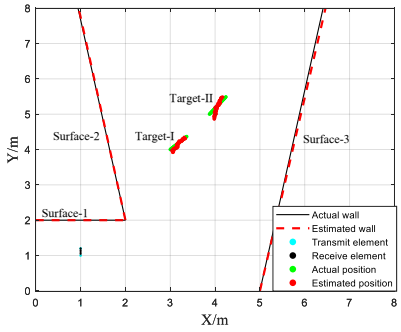

Fig. 5. Simulation results of two targets moving along straight routes.

its performance is evaluated only in terms of localization accuracy. The comparison results show an RMSE of 0.07 m over 50 frames. However, redundant ghosts can be observed, negatively impacting target detection performance. In contrast, the proposed algorithm not only improves localization accuracy but also enables effective building layout reconstruction, demonstrating its broader applicability.

To further assess the robustness of the proposed algorithm, 100 Monte Carlo experiments are conducted to evaluate parameter estimation performance under different SNR conditions. As shown in Fig. 4(a), the proposed method maintains stable performance across various SNR levels, whereas the performance of the GMM method significantly deteriorates at lower SNRs. In addition, the relationship between the building layout estimation results and the SNR is shown in Fig. 4(b). The results indicate that the proposed algorithm effectively estimates building layout parameters even in low-SNR environments, demonstrating strong robustness.

B. Two Targets Move Along Straight Routes

To further verify the feasibility of the proposed method in multi-target scenarios, a simulation experiment involving two targets is conducted. Assume that one target moves along a straight path from (3.00 m, 4.00 m) to (3.37 m, 4.37 m), while another target moves from (3.88 m, 5.00 m) to (4.24 m, 5.49 m). The proposed method enables separate target localization and building layout reconstruction for both targets, with the results presented in Fig. 5. To obtain the final estimation, the mean value of the building layout parameters derived from the estimation of each target is taken as the overall result. At an SNR of 20 dB, the RMSE for target 1 over 50 frames is 0.06 m, while for target 2, it is 0.10 m. The LOS wall position is estimated at 5.01 m, with a RMSE of 0.01 m. The LOS wall angle is 79.63°, with an RMSE of 0.37°, while the NLOS wall angle is 80.13°, with an RMSE of 0.13°. Considering that the target in the EM simulation experiment is a metallic cylinder with a radius of 0.20 m, such an RMSE appears reasonable.

V. Conclusion

In this paper, we propose a novel joint estimation algorithm for NLOS target localization and building layout reconstruction, aiming to mitigate the limitations of existing methods that rely on prior environmental knowledge. The algorithm integrates RD spectral topological feature extraction for TOA estimation and the IAA for DOA estimation, enabling accurate multipath ghost localization. Additionally, the spatial matching process ensures precise localization and layout reconstruction. EM simulations confirm that the proposed method improves target localization accuracy and demonstrates robustness in complex building environments.

References

[1] S. Sun, A. P. Petropulu, and H. V. Poor, "Mimo radar for advanced driver-assistance systems and autonomous driving: Advantages and challenges," *IEEE Signal Process Mag.*, vol. 37, no. 4, pp. 98 117, 2020.

[2] J. Jung, S. Lim, J. Kim and S. Kim, "Non-Line-of-Sight Vital Sign Detection Using Multipath Propagation of UWB Radar," *IEEE Antennas Wirel. Propag. Lett.*, vol. 23, no. 7, pp. 2219-2223, July. 2024.

[3] M. Gustafsson, Å. Andersson, T. Johansson, S. Nilsson, A. Sume and A. Örbom, "Extraction of Human Micro-Doppler Signature in an Urban Environment Using a "Sensing-Behind-the-Corner" Radar," *IEEE Geosci. Remote Sens. Lett.*, vol. 13, no. 2, pp. 187-191, Feb. 2016.

[4] B. -H. Pham, O. Rabaste, J. Bosse, I. Hinostroza, and Thierry Chonavel, "'Around-the-Corner' Radar: Particle Filters for Non-Line-of-Sight Target Tracking in the Presence of Ambiguities," *IEEE Trans. Aerosp. Electron. Syst.*, pp. 1–15, Jan. 2024.

[5] Q. Tang, J. Li, L.Wang, Y. Jia and G. Cui, "Multipath Imaging for NLOS Targets Behind an L-Shaped Corner with Single-Channel UWB Radar," *IEEE Sens. J.*, vol. 22, no. 2, pp. 1531-1540, Jan. 2022.

[6] H. Du, C. Fan, Z. Chen, C. Cao, and X. Huang, "NLOS Target Localization with an L-Band UWB Radar via Grid Matching," *Prog. In Electromagn. Res.*, Vol. 97, 45-56, 2020.

[7] J. Chen et al., "Joint Estimation of NLOS Building Layout and Targets via Sparsity-Driven Approach," *IEEE Trans. Geosci. Remote Sensing*, vol. 60, pp. 1–13, 2022.

[8] S. Xue et al., "NLOS Building Layout and Target Estimation in an L-Shaped Corner With Complex Geometries," *IEEE Trans. Instrum. Meas.*, vol. 74, pp. 1–12, 2025.

[9] Z. Xu, S. Guo and J. Chen et al., "Multi-Domain Features-Based NLOS Target Localization Method for MIMO UWB Radar," *IEEE Sens. J.*, vol. 23, no. 23, pp. 29314-29322, Dec. 2023.

[10] T. Yardibi, J. Li, P. Stoica, M. Xue, and A. B. Baggeroer, "Source localization and sensing: A nonparametric iterative adaptive approach based on weighted least squares," *IEEE Trans. Aerosp. Electron. Syst.*, vol. 46, no. 1, pp. 425–443, Jan. 2010.

[11] S. Fan, G. Cui, S. Guo, L. Kong, X. Yang, and X. Yuan, "Corner target positioning with unknown walls' positions," *J. Eng.*, vol. 2019, no. 19, pp. 6143–6146, Jul. 2019.

[12] C. Warren, A.Giannopoulos, and I. Giannakis, "gprmax: Opensource software to simulate electromagnetic wave propagation for ground penetrating radar," *Comput. Phys. Commun.*, vol. 209, pp. 163–170, 2016.

[13] T. Chai and R. R. Draxler, "Root mean square error (RMSE) or mean absolute error (MAE)? – Arguments against avoiding RMSE in the literature," *Geosci. Model. Dev.*, vol. 7, no. 3, pp. 1247–1250, Jun. 2014.